Hindawi Publishing Corporation
Mathematical Problems in Engineering
Volume 2007, Article ID 81514, 24 pages
doi:10.1155/2007/81514

Research Article

Successive Bifurcation Conditions of a Lorenz-Type Equation for the Fluid Convection Due to the Transient Thermal Field

Xiaoling He

Received 13 October 2006; Revised 13 February 2007; Accepted 7 June 2007

Recommended by José Manoel Balthazar

This paper investigates the convection flow between the two parallel plates in a fluid cell subject to the transient thermal field. We use the modal approximations similar to that of the original Lorenz model to obtain a generalized Lorenz-type model for the flow induced by the transient thermal field at the bottom plate. This study examines the convection flow bifurcation conditions in relation to the transient temperature variations and the flow properties. We formulated successive bifurcation conditions and illustrated the various flow behaviors and their steady-state attractors affected by the thermal field functions and fluid properties.

1. Introduction

The study of the thermally induced convection flow, or the Rayleigh-Benard convection problem, has centered on the Lorenz equation since 1963 when Lorenz used the 3-mode truncation of the Fourier series to obtain a nonlinear model [1]. Lorenz used the Boussinesq approximation adopted by Saltzman [2] who solved the convection flow problem in a seven-mode Fourier series approximation. The Lorenz equation represents the Rayleigh-Benard convection for both the parallel and circular plates [3, 4]. Essentially, the Boussinesq approximation originates from the Navier-Stokes equation and the heat conduction equation when the variation of the fluid density is negligible. The Lorenz model concerns the thermally induced convection flow by a steady-state temperature difference between the two parallel plates. Lorenz's simplification to the nonlinear equation allows for identification of the convection flow characteristics, such as the strange attractors and flow stabilities. Major investigations of the Lorenz system have been on the

bifurcation, stability, and chaos at different Rayleigh numbers and at both the small and large Prandtl numbers [5–8]. These earlier studies are largely based on numerical computations or experimental observations, which demonstrate various behaviors, including the sequential bifurcations with respect to the Rayleigh numbers and chaos with sensitive dependence on the initial conditions. In addition, both the homoclinic and heteroclinic bifurcations occur leading to periodic orbits [9–11]. The study by McLaughlin found that the sequential bifurcation of the Lorenz system itself can give rise to chaos [12, 13]. Curry observed that chaos also persists when the system is subject to a harmonic forcing [14]. However, a formulation to explain the sequential bifurcations has not been well established yet.

A sustained interest in the nonlinear convection flow extends the nonlinear model further to higher order systems than the Lorenz three-dimensional model. Curry subsequently expanded the Lorenz model to a generalized Lorenz model of 14 modes. Curry found different bifurcation and stability conditions with this high-dimensional analogue of the convection flow problem [15]. Specifically, Curry's computation results indicate that a torus of a periodic orbit appeared at a higher r with period doubling bifurcations, where r is the ratio between the Rayleigh number and the critical Rayleigh number. Curry showed that the stability of the origin gives its way to the Hopf bifurcation at a critical Rayleigh number. This critical number r differs from that established from the original Lorenz model. In a separate study, Boldrighini and Franceschini [16] and Franceschini and Tebaldi [17] investigated a five-term truncation of the convection equations. They found that the system has a four-fold symmetry with four stable points and undergoes both Hopf bifurcation and the period doubling bifurcation at large Rayleigh numbers to produce four stable periodic orbits. Further, saddle node bifurcations exist at a larger r. Gibbon and McGuinness studied another variation of the five-mode truncation of the fluid convection model [18]. Their stability condition renders the Hopf bifurcation at $r = 1$ and bifurcations into nonstable torus at a high r, which is consistent with Curry's results. In general, the numerical computation results of the high-dimensional convection flow reveal a different stability and bifurcation condition from that of the original Lorenz model. It is apparent that such a deviation comes from the different modal truncations. For the Fourier series, although a higher order truncation gives a closer approximation of the system, the fundamental mode plays a dominant role compared with other modes. This makes the low-dimensional system, such as the Lorenz model, remain a valid approximation.

In spite of all the attention paid to the Lorenz system, major efforts have focused on a thermal field defined the same as that in the original Rayleigh's description, that is, a constant temperature difference between the two parallel plates is maintained externally [3]. This restriction excluded the transient thermal process in the plate. Therefore, the conclusions drawn from the Lorenz equation or a generalized higher-dimensional Lorenz-type model become invalid when a transient thermal field is present. The nonuniform transient temperature difference arises from a thermal and fluid energy transfer without external thermal modulation. Therefore, a formulation taking into account the nonuniform transient thermal field will better explain the relevant flow behaviors.

In this paper, we investigate the Rayleigh-Benard convection problem with a transient thermal field at the bottom layer. We derive the equation of motion with a transient thermal field using the same truncation modes as that of Lorenz. Our purpose for this study is to see how the transient thermal field influences the flow behavior, such as the bifurcation and chaos with respect to the Rayleigh number and fluid properties. We will answer questions on the sequential bifurcations to convection flow attractors and flow stability in quantified terms to justify the numerical computation results from prior models and from the current model. The study could reveal the difference and analogy between the original Lorenz system and the system with a nonuniform transient thermal field.

This paper is organized as follows. Subsequent to this introduction on the previous study of the original and the generalized Lorenz system, we derive the convection flow model with a nonuniform transient thermal field. Next, we examine the steady-state attractors of the flow subject to different thermal fields. In this part, we formulate various bifurcation conditions, such as the Hopf bifurcation, period doubling, and saddle node bifurcations that affect the attractor behavior and stability. In the fourth section, we illustrate the numerical computation results for the sequential bifurcations and the transient response behavior. We pay special attention to the homoclinic bifurcations at large r and offer our explanation of the phenomena. This paper concludes with discussions and a summary of the influence of a transient thermal field on flow behaviors.

2. The model

The flow within a parallel plates with a transient heat source at the bottom layer is shown in Figure 2.1. The flow is parallel in the y-direction. The flow velocity u, w in the horizontal x- and the vertical z-direction, respectively, are related to the stream function $\psi(x,z,t)$ by the continuity equation as

$$\frac{\partial u}{\partial x}+\frac{\partial w}{\partial z}=0, \qquad u=-\frac{\partial \psi}{\partial z}, \qquad w=\frac{\partial \psi}{\partial x}. \tag{2.1}$$

Using the Boussinesq approximation, that is, the variation of the fluid density is negligible, the equilibrium equation for the flow field is [2]

$$\frac{\partial u}{\partial t}+u\frac{\partial u}{\partial x}+w\frac{\partial u}{\partial z}+\frac{\partial P}{\partial x}-\nu\nabla^2 u=0, \tag{2.2a}$$

$$\frac{\partial w}{\partial t}+u\frac{\partial w}{\partial x}+w\frac{\partial w}{\partial z}+\frac{\partial P}{\partial z}-g\varepsilon T_1-\nu\nabla^2 w=0, \tag{2.2b}$$

$$\frac{\partial T}{\partial t}=-u\frac{\partial T}{\partial x}-w\frac{\partial T}{\partial z}+\kappa\nabla^2 T, \tag{2.3}$$

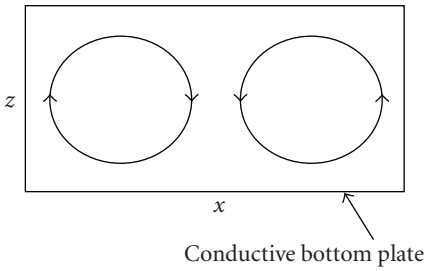

Figure 2.1. A flow field in two parallel plates.

where the thermal field is defined as

$$\begin{aligned} T(x,z,t) &= T_1(x,z,t) + \theta(x,z,t) = \left(1 - \frac{z}{H}\right)\Delta T + \theta(x,z,t), \\ T_1(x,z,t) &= \Delta T(x,0,t) - \frac{\Delta T(x,0,t)z}{H}, \\ \theta(x,z,t) &= \theta_{11}(x,z,t) + \theta_{02}(z,t). \end{aligned} \tag{2.4}$$

The laminate temperature variation is independent of the cell height, that is,

$$\frac{\partial \Delta T}{\partial z} = 0. \tag{2.5}$$

$\theta(x,z,t)$ is the transient temperature variation of the of the flow field, which is composed of the 2D variation $\theta_{11}(x,z,t)$ and the vertical variation $\theta_{02}(z,t)$, respectively. $\Delta T(x,0,t)$ is the temperature difference between the two parallel plates or equivalently the temperature variation of the bottom plate when the upper plate is as the reference. $\Delta T(x,0,t)$ causes a linear temperature variation along the vertical direction, $T_1(x,z,t)$. $\Delta T(x,0,t)$ has both transient and nonuniform spatial variations in the x-direction, that is, $\partial \Delta T(x,0,t)/\partial t \neq 0$, $\partial \Delta T(x,0,t)/\partial x \neq 0$.

Introducing (2.1) into (2.2a) and (2.2b), the governing equation of motion for the thermally induced convection flow is transformed to be

$$\frac{\partial}{\partial t}(\nabla^2\psi) - \frac{\partial \psi}{\partial z}\frac{\partial}{\partial x}(\nabla^2\psi) + \frac{\partial \psi}{\partial x}\frac{\partial}{\partial z}(\nabla^2\psi) - g\varepsilon\frac{\partial T_1}{\partial x} - \nu\nabla^4\psi = 0. \tag{2.6}$$

Here, g and ε are the gravitational acceleration and the coefficient of volume expansion of the fluid. With both spatial and temporal variations of the temperature, (2.3) becomes

$$\frac{\partial \theta}{\partial t} + \left[\left(\frac{\kappa}{\kappa_L} - 1\right)\frac{z}{H}\right]\frac{\partial \Delta T}{\partial t} = -\frac{\partial \theta}{\partial z}\frac{\partial \psi}{\partial x} + \frac{\partial \theta}{\partial x}\frac{\partial \psi}{\partial z} - \frac{z}{H}\frac{\partial \Delta T}{\partial x}\frac{\partial \psi}{\partial z} + \kappa\nabla^2\theta + \frac{\Delta T}{H}\frac{\partial \psi}{\partial x}. \tag{2.7}$$

The Rayleigh number is a function of the temperature difference between the two parallel plates, that is,

$$R_a = \frac{g\varepsilon H^3 \Delta T(x,z,t)}{\kappa\nu}. \tag{2.8a}$$

The critical Rayleigh number is

$$R_c = \frac{\pi^4}{a^2}\left(1+a^2\right)^3. \tag{2.8b}$$

$R_c = 27\pi^4/4$ when the convection occurs at a wave length of $a^2 = 1/2$ [2]. Considering the transient conductive thermal field in the form $\Delta T(x,t) = \Delta T(x) * g_T(t)$, the ratio between the two Rayleigh numbers r is

$$r(t) = \frac{R_a}{R_c} * g_T(t) = r * g_T(t). \tag{2.8c}$$

The function $g_T(t)$ represents the transient temperature variation with respect to time of a conductive plate. For example, $g_T(t)$ is an exponential function arising from solution of the diffusion equation

$$\frac{\partial \Delta T}{\partial t} = \kappa_L \nabla^2(\Delta T). \tag{2.9}$$

$g_T(t)$ can also assume other forms for different thermal processes in the solids.

By incorporating (2.9) for the heat conduction of the plate along with the heat conductivities at the boundaries, such as the Newmann or Dirichlet boundary conditions as explained below, we obtain a Lorenz-type model with a nonuniform transient thermal field as

$$\begin{aligned}
\frac{dX}{d\tau} &= -\sigma X + \sigma Y,\\
\frac{dY}{d\tau} &= cXZ - Y + rX,\\
\frac{dZ}{d\tau} &= drX + XY - bZ + e_\kappa r\beta,
\end{aligned} \tag{2.10a}$$

where

$$\begin{gathered}
\sigma = \frac{\nu}{\kappa}, \qquad \beta = \frac{g_{T,\tau}}{g_T}, \qquad b = \frac{4}{1+a^2}, \qquad c = 2\cos\left(\frac{2\pi z}{H}\right),\\
e_\kappa = \frac{1}{2}\left(\frac{\kappa}{\kappa_L} - 1\right)\left[1 + \frac{1}{2}\left(\frac{\pi z}{H}\right)^2\right].
\end{gathered} \tag{2.10b}$$

Note that here $g_{T,\tau}$ means $\partial g_T(\tau)/\partial\tau$. We adopted the same truncation modes X, Y, Z as that in the original Lorenz equation, which are dimensionless functions of the normalized time $\tau = (\pi/H)^2(1+a^2)\kappa t$ alone. The parameters b, σ, κ, ν, τ are defined the same as in

the original Lorenz equation, that is, the geometry factor b, Prandtl number σ, kinematic thermal viscosity ν, and thermal diffusivity of the fluid κ and that of the solid κ_L. It is worth mentioning that our derivation verified that the original Lorenz model represents the points of $z = H/3$ or $z = 2H/3$ only of the 2-dimensional flow field by assuming that $c = -1$ based on the expression $c = 2\cos(2\pi z/H)$ of this model.

In the above derivation, a series approximation is used for the temperature variation $\Delta T(x)$ with respect to x, in order to be consistent with the form of the functions X, Y, Z for the purpose of reduction. This variation of $\Delta T(x)$ introduces the thermal parameter d, which is related to heat conduction at the boundaries as follows:

(a) the von Neumann condition $\Delta T(x) = T_0 \sin(2\pi x/L)$ satisfies $\Delta T(x = 0,\ x = L) = 0$,

$$\begin{aligned} \Delta T(x,t) &= \Delta T(x) g_T(\tau), \\ d = d_N(x) &= -2\sqrt{2}\left(\frac{\pi x}{L}\right)^2, \quad d_N = \left[-2\sqrt{2}\pi^2, 0\right] = [-27.92, 0]. \end{aligned} \tag{2.11a}$$

(b) the Dirichlet condition $\Delta T(x) = T_0 \cos(2\pi x/L)$ satisfies $\partial \Delta T/\partial x(x = 0,\ x = L) = 0$,

$$\begin{aligned} \Delta T(x,t) &= \Delta T(x) g_T(\tau), \\ d = d_D(x) &= -\frac{\sqrt{2}\pi x}{L}, \quad d_D = \left[-\sqrt{2}\pi, 0\right] = [-4.44, 0]. \end{aligned} \tag{2.11b}$$

At the center of the plate $x = L/2$, $d_N|_{x=L/2} = -6.98$, $d_D|_{x=L/2} = -2.22$, $d_N = d_D|_{x=L/2\pi} = -\sqrt{2}/2$.

By incorporating the nonuniform transient thermal field, we obtain this Lorenz-type model that differs from the original Lorenz equation. The model correlates the convective flow with the transient temperature fluctuation function $\beta(\tau)$ in the conductive plate, the spatial temperature variation and the thermal boundary condition of the plate $d(x)$, and the plate-fluid thermal diffusion rate parameter $e_\kappa(z)$, respectively. The transient thermal field acts as a forcing source in the form $\beta(\tau) = g_{T,\tau}(\tau)/g_T(\tau)$, which measures the rate of change of the temperature or the thermal fluctuation of the plate. $\beta(\tau)$ drives the vertical temperature of the fluid Z directly to influence the flow field stream function X and the temperature variation Y. When $\beta(\tau) = 0$ and $d(x) = 0$, this model reduces to that by Lorenz.

As the definition entails, $e_\kappa(z)$ concerns the thermal diffusion between the fluid and the plate; $e_\kappa(z)$ influences the vertical temperature variation Z due to the heat exchange between the plate and the fluid. Since the thermal diffusivity of the fluid is generally greater than that of the solid, that is, $\kappa > \kappa_L$, therefore, $e_\kappa(z) > 0$. In addition, $e_\kappa(z)$ increases as the fluid-solid heat exchange rate subsides at the high end of the cell. As an example, the glycerin has conductivity in the range of $\kappa = 0.14$ [W/cm K], engine oil has $\kappa = 0.28$ [W/cm K], and a conductive metal plate has $\kappa = 0.2$ [W/cm K]. If $\kappa/\kappa_L = 5$ for the solid layer, $e_\kappa|_{\min} = 2$ at $z = 0$, and $e_\kappa|_{\max} = 11.89$ at $z = H$. At the same points for $c = -1$, that is, $z = H/3$ and $z = 2H/3$, $e_\kappa(z = H/3) = 3.08$ and $e_\kappa(z = 2H/3) = 6.38$, respectively.

This expanded model has the same negative divergence as the original Lorenz system, when the transient function $\beta(\tau)$ is considered as an external forcing, that is,

$$\frac{\partial \dot{X}}{\partial X} + \frac{\partial \dot{Y}}{\partial Y} + \frac{\partial \dot{Z}}{\partial Z} = -(1 + b + \sigma) < 0, \tag{2.12}$$

which suggests that the flow is dissipative. Geometrically, a dissipative system has all trajectories confined when the transient temperature rise is restricted. On the other hand, a rapid temperature rise certainly will cause oscillation without bound if $\beta(\tau)$ is unbounded.

3. The steady-state attractors and bifurcations

We examine the linearized system for the stability of the flow at the steady state, that is,

$$J = \begin{bmatrix} -\sigma & \sigma & 0 \\ cZ + r & -1 & cX \\ dr + Y & X & -b \end{bmatrix}. \tag{3.1}$$

3.1. The steady state at the origin for $X = Y = Z = 0$. The eigenvalues determine the stability and bifurcation behaviors of the system. For a steady-state attractor appearing at $X = Y = Z = 0$, the eigenvalues are given by

$$(\lambda + b)\big[(\lambda + 1)(\lambda + \sigma) - \sigma r\big] = 0. \tag{3.2}$$

It is evident that the eigenvalues are independent of $d(x)$ and the thermal fluctuation function $\beta(\tau)$. This defines the same eigenvalues as the Lorenz model, that is,

$$\begin{aligned} \lambda_1 &= -b < 0, \\ \lambda_{2,,3} &= \frac{1}{2}\Big[-(1+\sigma) \pm \sqrt{(1-\sigma)^2 + 4\sigma r}\Big] \\ &= \frac{1}{2}\Big[-(1+\sigma) \pm (1-\sigma)\sqrt{1+\delta}\Big], \quad \delta = \frac{4\sigma r}{(1-\sigma)^2} > 0. \end{aligned} \tag{3.3}$$

Using the series approximation,

$$\lambda_2 = \sigma\left[-1 + \frac{r}{(1-\sigma)}\right], \qquad \lambda_3 = -\left[1 + \frac{\sigma r}{(1-\sigma)}\right]. \tag{3.4}$$

$\lambda_2 < 0$ for $\sigma > 1$or $r < (1 - \sigma)$. Note that $\sigma > 1$ is a typical condition for the convection flow problem. $\lambda_3 < 0$ when $r > (1 - 1/\sigma)$. The negative eigenvalues produce a stable flow to the nodal attractor at the origin. The condition for the onset of the convection flow is $r < (1 - 1/\sigma)$. For $\sigma \to \infty$, this means that $r \to 1$.

An unstable saddle node bifurcation occurs at $\lambda_3 = 1$, corresponding to

$$r = 2\left(1 - \frac{1}{\sigma}\right). \tag{3.5}$$

This condition can be satisfied by numerous combinations of parameters, such as $\sigma = 2$, $r = 1$ and $\sigma = 10$, $r = 1.8$, which suggests that the system experiences a sequential saddle node bifurcation as r varies. In a similar fashion, we can find that the condition for period doubling bifurcation at $\lambda_1 = -b$ is $b = 1$. However, the period doubling bifurcation will not occur at $\lambda_{2,3} = -1$. This is because the physical parameter $r > 0$; $\lambda_2 = -1$ requires $r = -(1-\sigma)^2/\sigma < 0$ and $\lambda_3 = -1$ requires $r = 0$. Since all the eigenvalues are real, the steady state attractor at the origin does not undergo the Hopf bifurcation. However, a successive saddle node and period doubling bifurcations can occur at different r, b and σ.

3.2. The nonzero steady-state attractors. The steady-state attractor at the nonorigin, that is, at $X, Y, Z \neq 0$ is determined by $\dot{X} = \dot{Y} = \dot{Z} = 0$ from (2.10a), which yields

$$\begin{aligned} X &= Y, \\ cZ &= (1-r), \\ drX + X^2 - bZ + e_\kappa r\beta(\tau) &= 0. \end{aligned} \tag{3.6}$$

This defines the attractors at

$$\begin{aligned} X^2 + drX + \eta = 0, \quad \eta &= \frac{b}{c}(r-1) + e_\kappa r\beta(\tau) = \frac{1}{c}\left[r\left(b + ce_\kappa\beta(\tau)\right) - b\right], \\ X = Y &= \frac{1}{2}\left(-dr \pm \sqrt{(dr)^2 + \frac{4}{c}\left[b - r\left(b + ce_\kappa\beta(\tau)\right)\right]}\right), \\ Z &= \frac{1}{c}(1-r). \end{aligned} \tag{3.7}$$

The original Lorenz attractor at $c = -1$, $d = 0$, $e_\kappa = 0$ or $\beta(\tau) = 0$ is at

$$X = Y = \pm\sqrt{b(1-r)}, \qquad Z = r - 1. \tag{3.8}$$

X, Y can be either real or complex, depending on the value of r. To ensure the physical parameter X is a real parameter, the following condition should be satisfied:

$$\left(r^*\right)^2 - \frac{4b + 4ce_\kappa\beta(\tau)}{cd^2}r + \frac{4b}{cd^2} > 0. \tag{3.9}$$

For a real attractor X, Y, $r > r_1^*$ or $r < r_2^*$, $r_2^* < r_1^*$. The condition in (3.9) is alternatively expressed as

$$f_0(r^*) = \left(dr^*\right)^2 + \frac{4}{c}\left[b - r^*\left(b + ce_\kappa\beta(\tau)\right)\right] > 0. \tag{3.10}$$

The characteristic equation for the stability of the attractor is in the form

$$\lambda^3 + I\lambda^2 + II\lambda + III = 0, \tag{3.11}$$

where

$$\begin{aligned} I &= -(\lambda_1+\lambda_2+\lambda_3) = (1+b+\sigma), \\ II &= (\lambda_1\lambda_2+\lambda_1\lambda_3+\lambda_2\lambda_3) = b^2+b\sigma-cX^2, \\ III &= -\lambda_1\lambda_2\lambda_3 = \sigma cdrX, \end{aligned} \tag{3.12}$$

where X is determined by (3.7). The characteristics equation can lead to various bifurcation conditions determined by the eigenvalues, as we analyze below.

(a) *Periodic orbits with purely imaginary eigenvalues.* The steady-state attractors will not occur with a pair of purely imaginary eigenvalues. This is because the condition requires that

$$b+1=0. \tag{3.13}$$

As $b>0$, this is impossible. Similarly, it can be demonstrated that neither will a flow initiate due to the real eigenvalues of

$$\lambda_1=-b, \qquad \lambda_2=-\lambda_3. \tag{3.14}$$

(b) *All negative real eigenvalues and complex conjugacy.* For the Hopf bifurcation in a complex conjugacy $\lambda_{2,3}=\alpha\pm i\gamma$ and $\alpha=-1/2(I+\lambda_1)$, the coefficients of the characteristic equation become

$$\begin{aligned} I &= -(\lambda_1+2\alpha) = (1+b+\sigma), \\ II &= (2\alpha\lambda_1+\alpha^2+\gamma^2) = b^2+b\sigma-cX^2, \\ III &= -\lambda_1(\alpha^2+\gamma^2) = \sigma cdrX. \end{aligned} \tag{3.15}$$

For any $\alpha\lambda_1>0$ in either of the Hopf bifurcations, $II=2\alpha\lambda_1+\alpha^2+\gamma^2>0$. This defines the necessary condition associated with three possibilities: (a) all real eigenvalues to make $II>0$; (b) the subcritical Hopf bifurcation when $\alpha<0$ with $\lambda_1<0$; (c) the supercritical Hopf bifurcation when $\alpha>0$ with $\lambda_1>0$. However, $\alpha>0$ leads to $\lambda_1<-I<0$, since $I>0$ and $\alpha=-1/2(I+\lambda_1)$. Therefore, only cases (a) and (b) are possible. In the case of $\lambda_1=0$, $III=0$ and $X=0$. This means that there is no periodic orbit due to either of the Hopf bifurcations alone with $\lambda_1=0$. The condition $II>0$ generates the steady-state attractor at

$$X>-\frac{r(b+ce_\kappa\beta(\tau))-b+b(b+\sigma)}{cdr}=-\frac{(b+ce_\kappa\beta(\tau))}{cd}-\frac{b(b+\sigma-1)}{cdr}=\Delta_{nh}. \tag{3.16a}$$

For the steady-state response, this is equivalent to

$$f_{nh}(r)=\frac{1}{2}\left(-dr\pm\sqrt{(dr)^2+\frac{4}{c}[b-r(b+ce_\kappa\beta(\tau))]}\right)-\Delta_{nh}>0. \tag{3.16b}$$

Note that the condition (3.16) does not differentiate between cases of all real eigenvalues in $II>0$ and the case of complex conjugate eigenvalues with $\alpha<0$ and $\lambda_1<0$. This means that the necessary condition is not exclusive for either of the cases.

(c) *The Hopf bifurcation with complex eigenvalues.* In the case of the Hopf bifurcation with a real eigenvalues, we can further identify the necessary conditions for different cases. The condition can be expressed in the form identical to that in (3.16) except for the operator Δ_{nh}. That is,

$$f_j(r) = \frac{1}{2}\left(-dr \pm \sqrt{(dr)^2 + \frac{4}{c}\left[b - r\left(b + ce_\kappa\beta(\tau)\right)\right]}\right) - \Delta_j. \tag{3.17}$$

Here the function $f_j(r)$ is associated with the specific operator Δ_j, of which three conditions can be drawn based on the relation between λ_1 and α:

(1) $I * II - III < 0$, a necessary condition for the supercritical Hopf bifurcation with $\lambda_1 < -I < 0$, $\alpha > 0$, which requires the steady-state attractor to satisfies

$$X < -\frac{(1+b+\sigma)}{cdr(1+b)}\left[b(b+\sigma-1) + r\left(b + ce_\kappa\beta(\tau)\right)\right] = \Delta_H^-. \tag{3.18a}$$

Therefore, the necessary condition is

$$f_{\text{sup}}^-(r) = \frac{1}{2}\left(-dr \pm \sqrt{(dr)^2 + \frac{4}{c}\left[b - r\left(b + ce_\kappa\beta(\tau)\right)\right]}\right) - \Delta_H^- < 0. \tag{3.18b}$$

(2) $I * II - III > 0$ for the subcritical Hopf bifurcation with $-I < \lambda_1 < 0$ and $-I/2 < \alpha < 0$, which is the opposite condition to that for the supercritical Hopf bifurcation with $\lambda_1 < -I < 0$. Therefore, the necessary condition is

$$f_{\text{sub}}^-(r) = \frac{1}{2}\left(-dr \pm \sqrt{(dr)^2 + \frac{4}{c}\left[b - r\left(b + ce_\kappa\beta(\tau)\right)\right]}\right) - \Delta_H^- > 0. \tag{3.19}$$

(3) $II^2 - 4I * III > 0$ for the subcritical Hopf bifurcation with $\lambda_1 > 0$, $\alpha < -I/2 < 0$, this defines

$$X < \frac{\left\{\left(b^2 + b\sigma - b + \left(ce_\kappa\beta(\tau) + b\right)r\right)^2 - c(dr)^2\left[\left(ce_\kappa\beta(\tau) + b\right)r - b\right]\right\}}{\left\{4(1+b+\sigma)\sigma - 2\left(b^2 + b\sigma - b + \left(ce_\kappa\beta(\tau) + b\right)r\right) + c(dr)^2\right\}cdr} = \Delta_{\text{sub}}^+. \tag{3.20a}$$

This leads to the necessary condition of

$$f_{\text{sub}}^+(r) = \frac{1}{2}\left(-dr \pm \sqrt{(dr)^2 + \frac{4}{c}\left[b - r\left(b + ce_\kappa\beta(\tau)\right)\right]}\right) - \Delta_{\text{sub}}^+ < 0. \tag{3.20b}$$

The above three conditions are exclusive necessary condition for each Hopf bifurcation.

(d) *The Hopf bifurcation concurrent with the saddle node/period doubling bifurcations.* When the real eigenvalue is specified, the necessary and sufficient condition can be uniquely defined for the Hopf bifurcation with a real eigenvalue. For example, the period doubling or saddle node bifurcation can occur at $\lambda_1 = -1$ and $\lambda_1 = 1$, respectively,

concurrent with the subcritical Hopf bifurcation. This is because $\alpha < 0$ as long as $\lambda_1 > -(1+b+\sigma)$. Therefore,

$$\alpha_{\lambda_1=1} = \frac{1}{2}[-I-1] = -\frac{1}{2}(2+b+\sigma), \qquad \alpha_{\lambda_1=-1} = \frac{1}{2}[-I+1] = -\frac{1}{2}(b+\sigma). \tag{3.21}$$

Notice that a combination of $\lambda_1 = \pm 1$ and $\alpha = 0$ for the purely imaginary eigenvalues is impossible since $\lambda_1 < -1$ at $\alpha = 0$.The necessary and sufficient condition for the Hopf bifurcation with any real λ_1 is

$$III + \lambda_1 II = -(\lambda_1)^2(I+\lambda_1), \tag{3.22}$$

which defines the attractor at

$$X = -\frac{\{(\lambda_1)^2(1+\sigma+b+\lambda_1) + \lambda_1[b^2+b\sigma-b+r(b+ce_\kappa\beta(\tau))]\}}{(\lambda_1+\sigma)cdr} = \Delta_H^*. \tag{3.23a}$$

Equivalently, this gives the bifurcation condition of:

$$f_H^*(r) = \frac{1}{2}\left(-dr \pm \sqrt{(dr)^2 + \frac{4}{c}[b-r(b+ce_\kappa\beta(\tau))]}\right) - \Delta_H^* = 0. \tag{3.23b}$$

The condition in (3.22) ensures that all the necessary conditions for the Hopf bifurcation in (3.18), (3.19), and (3.20) are satisfied. For example, in the case of the supercritical Hopf bifurcation with $\lambda_1 < -I < 0$, the condition $I * II - III < 0$ becomes

$$\begin{aligned} I * II - III &= I * II + \lambda_1^- II + (\lambda_1^-)^2 I + (\lambda_1^-)^3 < I * II - I * II + (\lambda_1^-)^2 I + (\lambda_1^-)^3 \\ &= (\lambda_1^-)^2[I + (\lambda_1^-)] < 0. \end{aligned} \tag{3.24a}$$

For the subcritical Hopf bifurcation with $-I < \lambda_1 < 0$, $\alpha < 0$, $I * II - III > 0$ is satisfied by

$$\begin{aligned} I * II - III &= I * II + \lambda_1^- II + (\lambda_1^-)^2 I + (\lambda_1^-)^3 > I * II - I * II + (\lambda_1^-)^2 I + (\lambda_1^-)^3 \\ &= (\lambda_1^-)^2[I + (\lambda_1^-)] > 0. \end{aligned} \tag{3.24b}$$

For the subcritical Hopf bifurcation with $\lambda_1 > 0$, $\alpha < 0$, the condition $II^2 - 4I * III > 0$ is

$$II^2 + 4I * (\lambda_1^- II + (\lambda_1^-)^2 I + (\lambda_1^-)^3) = [II + 2(\lambda_1^- I)]^2 + 4(\lambda_1^-)^3 * I > 0. \tag{3.24c}$$

The condition (3.23) can also determine the concurrent saddle node bifurcation at $\lambda_1 = 1$ and the period doubling bifurcation at $\lambda_1 = -1$, respectively, since, (3.23) is the necessary and sufficient condition for the Hopf bifurcations with a specified eigenvalue. This condition defines the Hopf bifurcation curve, whereas those necessary conditions in (3.18), (3.19), and (3.20) define the domain boundaries for the bifurcation they are associated with. These conditions describe a bifurcation map with respect to the physical parameters. The fact that all of the conditions are in the third order polynomials of r

suggests that several ranges of parameters could coexist to satisfy the condition. As a result, the system exhibits sequential bifurcations discussed above. One exception is the Hopf bifurcation with a pair of purely imaginary eigenvalues, which will not occur due to the restriction of the physical parameters. These bifurcation conditions provide qualified and quantified terms to define the steady-state attractors and describe their stability due to various bifurcations.

4. Computation results

We use a numerical computation in the 4th-order Runge-Kutta method to study the bifurcation behavior and the response of the system. We fixed parameters at $c = -1$, $d = -\pi$ for the response with respect to σ, b, and r.

4.1. Bifurcation conditions. The computation for the bifurcation map assumes the fluid property parameters b and σ in the range of [0 10]. We study various bifurcation conditions that can be satisfied by the parameters in this range with respect to σ and b when r and $\beta(\tau)$ are specified. The purpose of the computation is to demonstrate the influence of the transient thermal field effect on the convective flow of the specified geometry loci. For the Hopf bifurcations with a specified eigenvalue λ_1, we select the period doubling bifurcation at $\lambda_1 = -1$ and the saddle node bifurcation at $\lambda_1 = 1$, respectively. In addition, the Hopf bifurcation conditions at both $\lambda_1 = 15$ and $\lambda_1 = -15$ are examined. At $\lambda_1 = -15$, either a supercritical or a subcritical Hopf bifurcation can occur since the real part of the complex conjugate α varies between $\alpha = -3$ and $\alpha = 7$ for b, σ in the range of [0 10]. For $\lambda_1 = 15$, only a subcritical Hopf bifurcation is possible as α varies between $\alpha = -8$ and $\alpha = -18$. These four curves are marked by fsd for the Hopf bifurcation with the saddle node, fpd for that with the period doubling, fHp for the subcritical Hopf bifurcation at $\lambda_1 = 15$ and fHn for the Hopf bifurcation at $\lambda_1 = -15$, respectively. Curves $f\,\mathrm{sub}\,p > 0$, $fh > 0$ and $fnh > 0$ represent the contour projections of the function $f^{+}_{\mathrm{sub}}(r) > 0$ in (3.20b), $f^{-}_{\mathrm{sub}}(r) > 0$ in (3.19), and $f_{nh}(r) > 0$ in (3.16b), respectively, for the three distinct necessary conditions associated with the Hopf bifurcations and other possible cases. Therefore, curves fsd, fpd, and fHn and fHp define the necessary and sufficient conditions while each other one represents the necessary condition only.

Figures 4.1(a), 4.1(c), and 4.1(e) show the bifurcation curves at a specified r and $\beta(\tau)$. Figure 4.1(a) is for $r = 5$ and $\beta(\tau) = 0$ whereas Figure 4.1(c) shows the bifurcation at $r = 5$ and $\beta(\tau) = -10$. In both figures, we observe the curve with the saddle node bifurcation, fsd, the curve with the period doubling fpd and the curve fHn for the Hopf bifurcation at $\lambda_1 = -15$. The curve $f\,\mathrm{sub}\,p > 0$ in Figure 4.1(a) defines parameter range that satisfies the condition for a successive subcritical Hopf bifurcation with $\lambda_1 > 0$. The 3D plot for the condition $f\,\mathrm{sub}\,p$ is shown in Figure 4.1(b), indicating that the intercepted area by the two blue curves satisfy $f\,\mathrm{sub}\,p > 0$. Curve fHp also appears in both Figures 4.1(a) and 4.1(c) for the subcritical Hopf bifurcation with $\lambda_1 = 15$, with different parameter ranges.

Note that there are two curves of $fh > 0$ for the subcritical Hopf bifurcation with $\lambda_1 < 0$, that is, $f^{-}_{\mathrm{sub}}(r) > 0$, in Figures 4.1(a) to 4.1(c), as a result of the projection at a specified value at $fh = 50$, similar to the curve $f\,\mathrm{sub}\,p > 0$ in Figure 4.1(a). For the case in Figure 4.1(c) with $r = 5$ and $\beta = -10$, the necessary condition $f^{-}_{\mathrm{sub}}(r) > 0$ in (3.17),

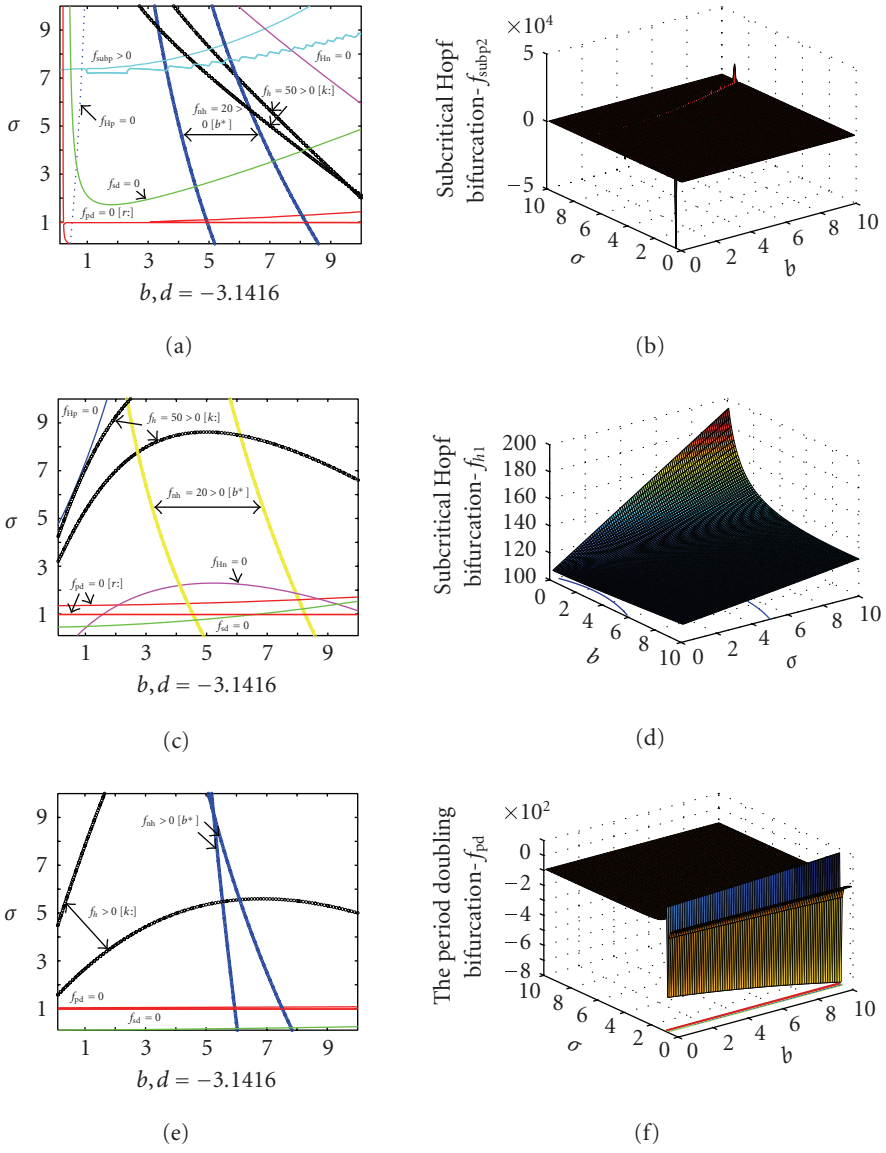

FIGURE 4.1. Bifurcation conditions and map. (a) Bifurcation map at $r = 5$, $\beta = 0$. (b) The subcritical Hopf bifurcation condition $f^{+}_{\text{sub}}(r) > 0$ at $r = 5$, $\beta = 0$. (c) Bifurcation map at $r = 5$. (d) The subcritical Hopf bifurcation condition with $\lambda_1 < 0$ $f^{-}_{\text{sub}}(r) > 0$ at $r = 28$. (e) Bifurcation map at $r = 28$. (f) Condition for the period doubling bifurcation at $f_{PD}(r)$ at $r = 28$.

shown by $fh = 50 > 0$, is uniformly satisfied by the parameters in the 2D domain as shown in Figure 4.1(d) for $f^{-}_{\text{sub}}(r) > 0$. The curves in Figures 4.1(a) and 4.1(c) illustrate only a selective projection of the contour at $fh = 50$. In both Figures 4.1(a) and 4.1(c), the necessary condition for $f_{nh}(r) > 0$ is also satisfied, marked by the curve $fnh > 0$ where

the projection is at $f_{nh}(r) = 20$ in Figure 4.1(a) and $f_{nh}(r) = 50 > 0$ in Figure 4.1(c). Both conditions $fh > 0$ for $f_{\text{sub}}^{-}(r) > 0$ and $fnh > 0$ for $f_{nh}(r) > 0$ are valid in the entire domain of b and σ in Figures 4.1(a) and 4.1(c).

The variation of $\beta(\tau)$ changes the bifurcation conditions as it is evident from comparison of Figures 4.1(a) and 4.1(c) where the same condition is satisfied by different parameters. In the same token, a different r also alters the bifurcation map. Figure 4.1(e) is the map for $r = 28$ and $\beta = -10$, where the Hopf bifurcation curve with the period doubling and the saddle node bifurcations are illustrated. The curves $fh > 0$ and $fnh > 0$ are again selective contour projections of functions that are satisfied by the parameters b, σ in the range of [0 10]. Figure 4.1(f) shows that the Hopf bifurcation concurrent with the period doubling bifurcation occurs around $\sigma = 1$, which is characteristic for all different range of parameters as seen from Figures 4.1(a), 4.1(c), and 4.1(e) also.

4.2. Transient thermal field functions. We study three different transient thermal field functions, which are as follows.

(a) *The harmonic function* $g_T(\tau)$. A cyclic function of $\beta(\tau)$ results. Specifically,

$$g_T(\tau) = \cos(\omega\tau), \qquad \beta(\tau) = -\omega\tan(\omega\tau)\begin{cases} < 0, & 0 < (\omega\tau) < \pi/2, \\ > 0, & \pi/2 < (\omega\tau) < \pi. \end{cases} \tag{4.1a}$$

Note that the sign of ω does not affect the sign of $\beta(\tau) = -\omega\tan(\omega\tau)$ in each bounded interval $k\pi < (\omega\tau) < (k+1)\pi + \pi/2$.The function $\beta(\tau)$ goes to infinity at the boundaries $(\omega\tau) = (k+1)\pi \pm \pi/2$. The function $\beta(\tau)$ causes instantaneous change of the attractors due to transitions of the bifurcation conditions, which makes the condition $\dot{X} = \dot{Y} = \dot{Z} = 0$ invalid. Equivalently, this suggests that a steady-state attractor at $\dot{X} = \dot{Y} = \dot{Z} = 0$ does not exist in this case.

(b) *The exponential function* $g_T(\tau)$ *for the thermal conduction.* The exponential function $g_T(\tau)$ produces a constant driving force as

$$g_T(\tau) = \exp(-\omega\tau), \qquad \beta(\tau) = -\omega. \tag{4.1b}$$

The function $\beta(\tau) > 0$, if $\omega < 0$ for a temperature rise or vice versa. Therefore, a temperature rise or decline for $\beta(\tau) > 0$ or $\beta(\tau) < 0$ will influence the steady state response in a different fashion. However, in each case the steady-state attractor, as defined in (3.7), remains stationary since $\beta(\tau)$ is a constant.

(c) *The linear function* $g_T(\tau)$. The linear function $g_T(\tau)$ makes $\beta(\tau) > 0$ and $\beta(\tau) \to 0$ as $\tau \to \infty$, that is,

$$g_T(\tau) = \omega\tau, \qquad \beta(\tau) = \frac{1}{\tau} > 0. \tag{4.1c}$$

The three transient thermal field functions $\beta(\tau)$ discussed above suggest that the steady state is not stationary with a harmonic function $g_T(\tau)$, while the exponential and linear functions lead to stationary attractors.

4.3. Transient responses. We use a time step $h = 0.001$ second to generate the transient response for steps of $N = 10,000$ for this system with respect to different $\beta(\tau)$ and other parameters. The initial condition is assumed to be $X = 0$, $Y = 20$, $Z = 10$, unless otherwise specified.

(a) $r = 1$, $\beta(\tau) = 0$, *nodal attractors at the origin.* For $r = 1$ and $\beta(\tau) = 0$ without the transient thermal effect, the response could converge to the steady-state $X = Y = 0$, $Z = r - 1$ or $X = Y = -d$, $Z = r - 1$, depending on the initial conditions. Figures 4.2(a) and 4.2(b) show that all X, Y, and Z converge to the zero steady-state attractor at $r = 1$, $b = 8/3$, $\sigma = 6.33$ with the given initial conditions. The steady state reaches the nodal point $X = 0$, $Y = 0$, $Z = 0$ quickly after a transient oscillation. The corresponding eigenvalues are all real and negative, that is, $\lambda = 0, -10.4273, -3.2394$, which makes the nodal attractor stable.

(b) $r = 5$, $\beta(\tau) = 0$, *the Hopf bifurcation.* The parameters $b = 8/3$, $\sigma = 10$, $r = 5$ induce the subcritical Hopf bifurcation with eigenvalues of $\lambda_1 = 11.5572$ and $\lambda_{2,3} = -12.6119 \pm 20.8298i$. Figures 4.2(c) and 4.2(d) show a spiral oscillation leading to the nonzero steady-state attractor. A similar behavior exists at $r = 28$, shown in Figures 4.2(e) and 4.2(f). A higher oscillation frequency during the transition to the steady-state is evident at $r = 28$ in comparison with that at $r = 5$, as shown in the phase diagrams of X-Y and Y-Z for $r = 5$ and $r = 28$, respectively. This is caused by the eigenvalue with an increased imaginary part at $r = 28$, which is $\lambda_1 = 23.6679$ and $\lambda_{2,3} = -18.7065 \pm 91.5255i$.

(c) $r = 28$ *with different transient thermal field functions.* The response behaves differently with a different transient thermal field function $\beta(\tau)$. Figures 4.3(a) and 4.3(b) show the transient response with $b = 8/3$, $\sigma = 10$, $r = 28$ and $\beta(\tau) = 1/\tau$. The transient response vanishes after certain iterations with the ensuing oscillation approaching the steady state by way of the Hopf bifurcation as $\beta(\tau) = \lim_{\tau\to\infty}(1/\tau) = 0$. The steady state attractor is identical to that shown in Figures 4.2(e) and 4.2(f), respectively.

The response with an exponential function $g(\tau) = \exp^{-(\pi/2)\tau}$ and $\beta(\tau) = (\pi/2)$ is shown in Figures 4.3(c) and 4.3(d) with $b = 8/3$, $\sigma = 10$, and $r = 28$. The transient exponential function, in fact, produces a constant driving force to the system. This function $\beta(\tau)$ directly influences the vertical temperature $Z(\tau)$ and modifies the attractor X, Y, and Z. The steady-state attractor is at $X = Y = 88.64$, $Z = 27$ for $\beta(\tau) = (\pi/2)$ shown in Figures 4.3(c) and 4.3(d) for the phase diagrams of X-Y and Y-Z, respectively. Note that the subcritical Hopf bifurcation produces a spiral for either $\beta(\tau) = (\pi/2)$ or $\beta(\tau) = 1/\tau$ approaching a stationary steady-state attractor. Notably, the attractor position Z is independent of $\beta(\tau)$, although $\beta(\tau)$ influences the transient behavior of Z prior to the steady state. Each initial response goes through a period of increasing amplitude for different r and different function $\beta(\tau)$. This is caused by the positive real eignevalue λ_1. Such increase is eventually balanced by the negative real part of the complex eigenvalues, which eventually makes the periodic oscillation dominate in a subcritical Hopf bifurcation.

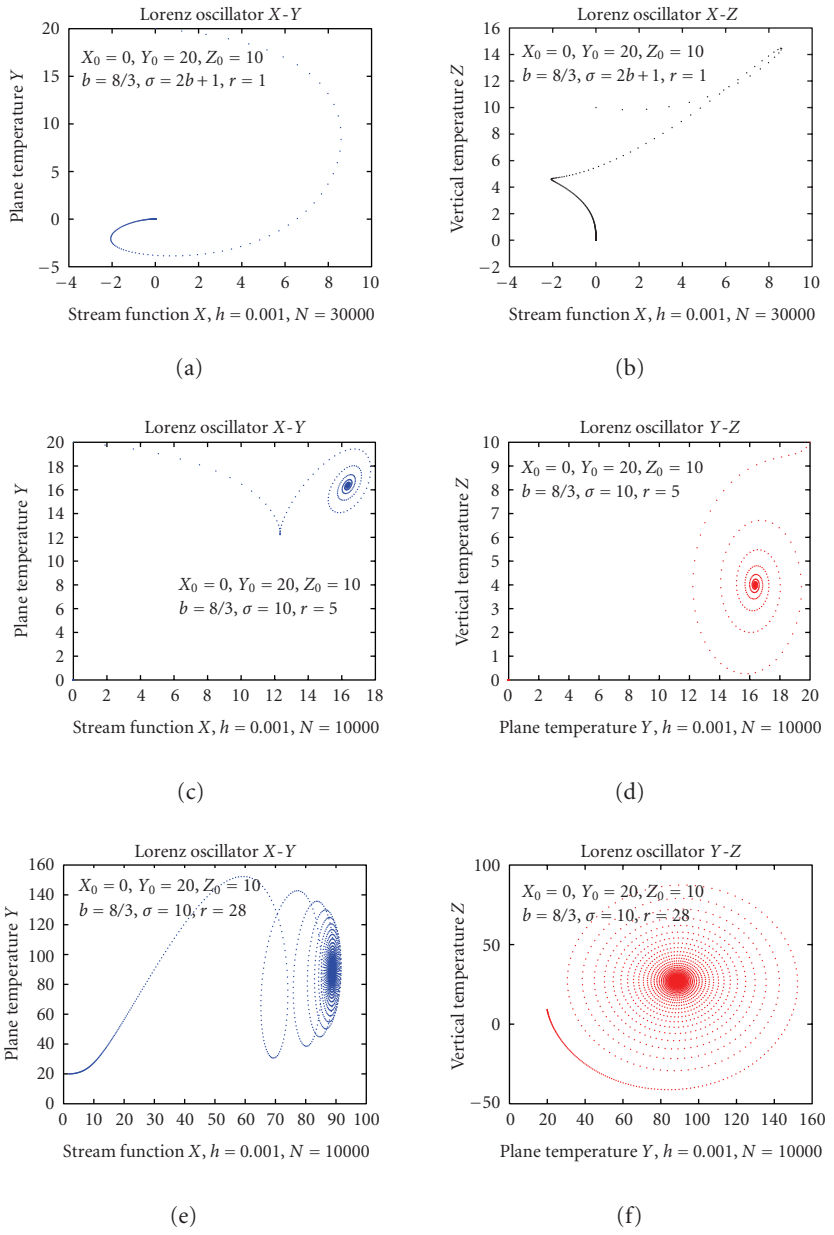

FIGURE 4.2. Phase diagrams without the transient effect. (a) X-Y at $b = 8/3$, $\sigma = 2b + 1$, $r = 1$. (b) X-Z at $b = 8/3$, $\sigma = 2b + 1$, $r = 1$. (c) X-Y at $b = 8/3$, $\sigma = 10$, $r = 5$. (d) Y-Z at $b = 8/3$, $\sigma = 10$, $r = 5$. (e) X-Y at $b = 8/3$, $\sigma = 10$, $r = 28$. (f) Y-Z at $b = 8/3$, $\sigma = 10$, $r = 28$.

The attractor's behavior with an assumed constant function $\beta(\tau)$ is an instant representation of the oscillatory attractors with a transient function $\beta(\tau)$, whereas the attractor

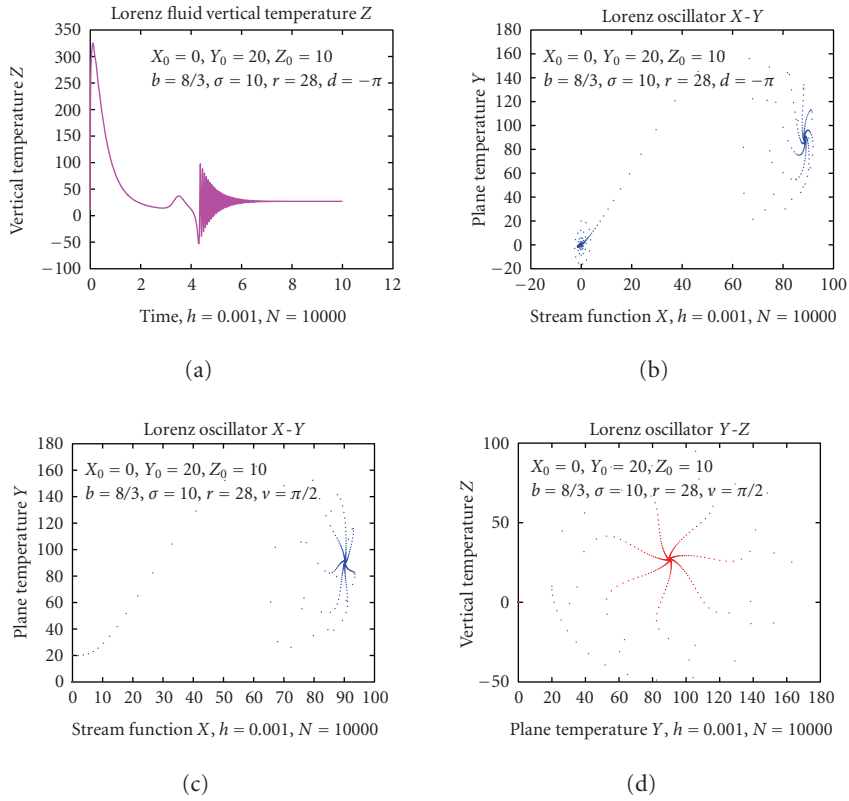

FIGURE 4.3. Response with a transient function $\beta(\tau)$, $b = 8/3$, $\sigma = 10$, $r = 28$. (a) Z versus time, $\beta(t) = 1/\tau$. (b) X-Y phase diagram, $\beta(t) = 1/\tau$. (c) X-Y phase diagran $\beta(t) = \pi/2$, $g(t) = \exp^{-(\pi/2)\tau}$. (d) Y-Z phase diagram, $\beta(t) = \pi/2$, $g(t) = \exp^{-(\pi/2)\tau}$.

experiences instantaneous oscillations with respect to the transient eigenvalues and function $\beta(\tau)$. The steady-state attractor also experiences instability when the function $\beta(\tau)$ approaches infinity such as in the case of $\beta(\tau) = -\omega \tan(\omega\tau)$. The oscillatory behavior of attractors associated with the transient function $\beta(\tau)$ means that the steady-state attractors can not be predicted based on the assumption of $\dot{X} = \dot{Y} = \dot{Z} = 0$, as that in (3.7). In fact, a steady-state attractor does not exist for a case of $\dot{X} \neq 0$, $\dot{Y} \neq 0$, $\dot{Z} \neq 0$.

(d) *The homoclinic bifurcation at* $r = 1000$*, a periodic oscillation.* In contrast with the bifurcation conditions associated with the steady-state attractors, another type of bifurcation occurs independent of these conditions, that is, the homoclinic explosion, a phenomenon that transform the steady-state oscillation to a newly born set of orbits. Figures 4.4(a) to 4.4(f) show a periodic oscillation as a result of the explosion at $b = 8/3$, $\sigma = 10$, $r = 1000$ and $\beta(\tau) = \pi$ with a transient function $g_T(\tau) = \exp^{-\pi\tau}$. The time history of X, Y and Z in Figures 4.4(a), 4.4(c), and 4.4(e), respectively, indicates a burst of the homoclinic explosion after the steady state is sustained for a certain period of time. The

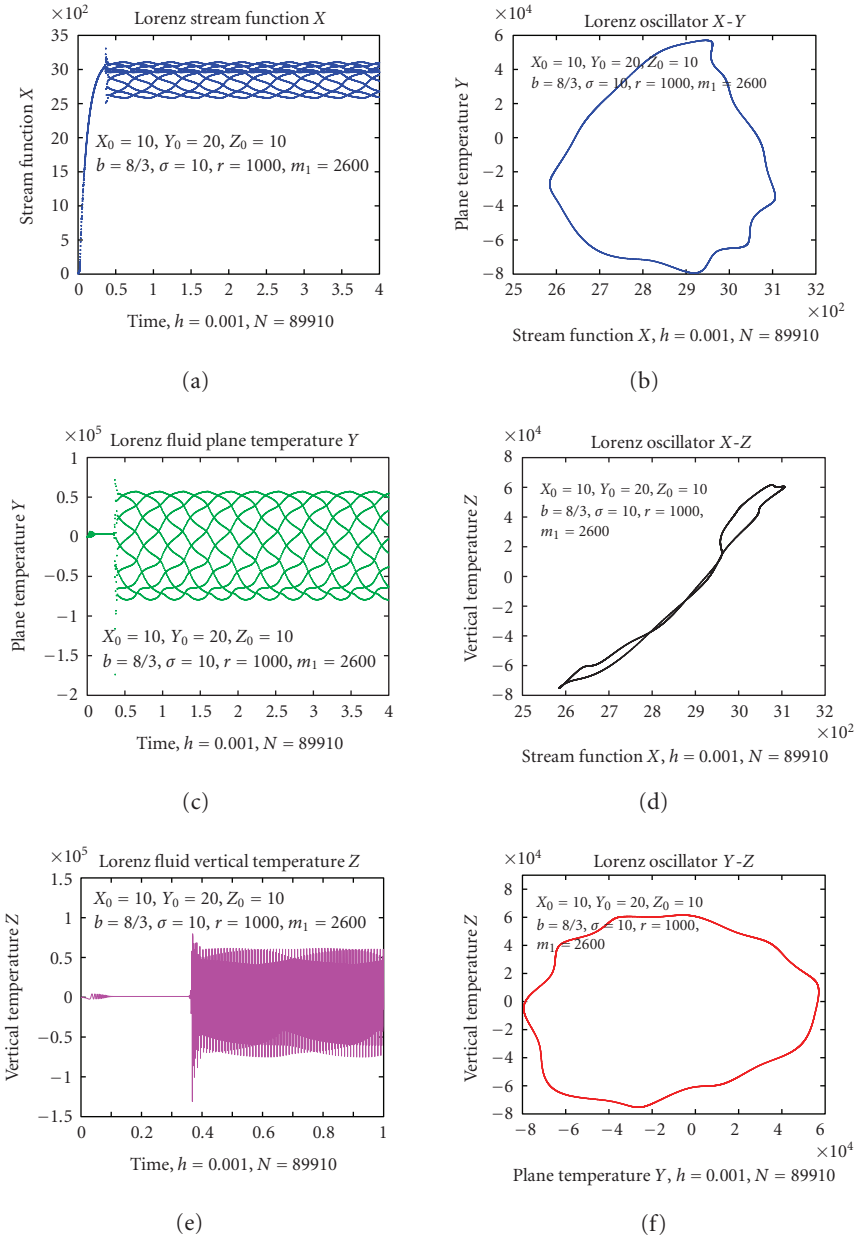

FIGURE 4.4. Response with a transient function $\beta(t) = \pi$, $b = 8/3$, $\sigma = 10$, $r = 1000$. (a) X versus time. (b) steady-state Poincare map X-Y. (c) Y versus time. (d) steady-state Poincare map X-Z. (e) Z versuss time. (f) steady-state Poincare map Y-Z.

Poincare maps shown in Figures 4.4(b), 4.4(d), and 4.4(f) are sampled at a frequency interval $\Delta h = 0.01$ s, equivalent to 10 iterations for each point. Totally 87,310 periodic

traces are taken in each map after eliminating the transient 2,600 iterations. These orbits remain the same as those with fewer sampling points, such as $N = 10{,}000$, or those at a different sampling frequency. These identical Poincare maps confirm that the orbit is periodic. The numerical computation results also reveal that the response with $\beta(\tau)$ from a linear transient function arrives at the same periodic orbit due to the explosion after reaching the steady state predicted by (3.7). $\beta(\tau)$ only influences the duration of the steady state prior to such an explosion, but not the orbit after the explosion.

(e) *The steady state at $r = 903$, a quasi-periodic oscillation.* Another bifurcation behavior exists, as can be observed from the phase diagrams at $b = 8/3$, $\sigma = 10$, and $r = 903$, where the homoclinic bifurcation leads to multiple periodic orbits. Figures 4.5(a), 4.5(c), and 4.5(e) show the bifurcation explosion after an initial steady-state sustained for about 2000 iterations. The phase diagrams in Poincare maps show a finite number of orbits in Figures 4.5(b), 4.5(d), and 4.5(f), after eliminating the initial 2600 transient iterations. Our extensive computation results verified that such a homoclinic bifurcation initiates at a higher Rayleigh number, that is, about $r = 900$. This transition number r is also affected by the exponential function frequency ω.

Figures 4.4 and 4.5 together suggest that the system experiences homoclinic bifurcations that lead to another steady state. This phenomenon agrees with the earlier observation from that of the original Lorenz model in that homoclinic explosions at a large r lead to periodic orbits [11]. Our results ascertain that such homoclinic explosions persist with different transient functions $\beta(\tau)$. Namely, a different $\beta(\tau)$ function leads to identical orbits as a result of the explosion, that is, either a monotonic periodic orbit or multiple period orbits.

There exists no valid explanation for such explosion phenomena that occur at a large r except consistent computation observations. However, examining the eigenvalues for each case suggests that cases with a large number r are associated with an insignificant real eigenvalues, that is, $\lambda_1 = 26.6$ at both $r = 1000$ and $r = 903$. At the same time, the complex conjugates have a trivial real part where the real and the imaginary part has a ratio in the order of 10^2, that is, $\lambda_{2,3} = -20.18 \pm 3139.10i$ for $r = 1000$; $\lambda_{2,3} = -20.16 \pm 2837.40i$ for $r = 903$, respectively. The steady-state attractors are at $X = 3138.9$, $Z = 999$ and $X = 2837.3$, $Z = 902$, respectively. These eigenvalues suggest that the amplitude of the steady-state oscillation is insignificant, due to the canceling effect between the real and the complex eigenvalues. Such a behavior is evident in the time history of the oscillation prior to the explosion. However, such trivial oscillation is subject to computing errors which can alter the eigenvalues and give birth to new periodic orbits. Therefore, the homoclinic orbit is a manifestation of the transition of eigenvalues as a result of the computation error perturbation. A single periodic oscillation is the consequence of a pair of stable eigenvalues due to such a perturbation, whereas a multiperiod oscillation occurs when the eigenvalues are unstable, experiencing multiple transitions among different values. Therefore, the phase diagram embodies either a finite number of periodic orbits when the eigenvalues are finite or an infinite number of orbits when the eigenvalues vary continuously. Although the function $\beta(\tau)$ influences the transient behavior, we observe that the initiation of the explosion is dependent on $\beta(\tau)$. The skew-shaped periodic orbit for the Poincare map in Figures 4.4(d) and 4.5(d) with $X \neq Y$ is the consequence of such perturbation

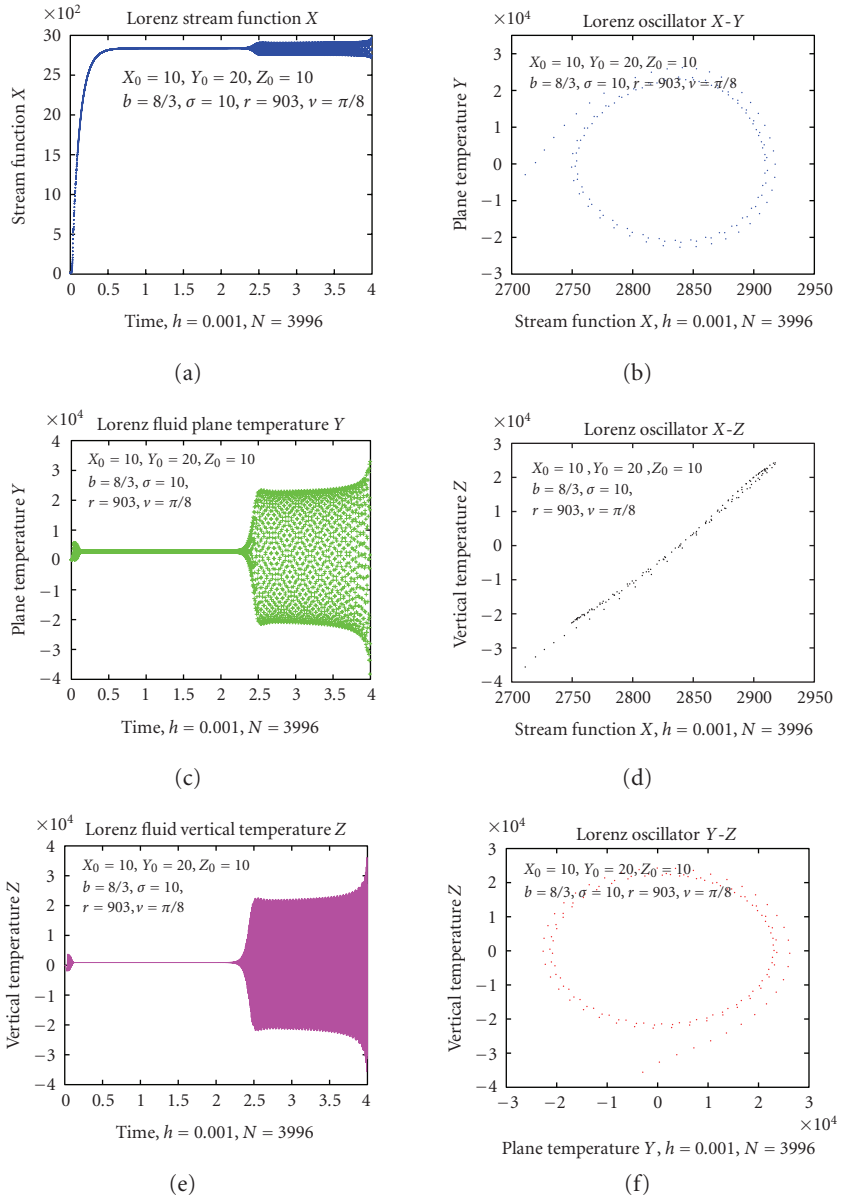

FIGURE 4.5. Response with a harmonic function $\beta(t) = -\nu\tan(\nu t)$, $b = 8/3$, $\sigma = 10$, $r = 903$, $\nu = \pi/8$. (a) X versus time. (b) Transient response Y versus time. (c) Z versus time. (d) steady-state Poincare map X-Y. (e) Steady-state Poincare map X-Z. (f) Steady-state Poincare map Y-Z.

that produces the orbits different from those predicted by the steady-state analysis. Another fact that can be verified from the expression of the coefficients in (3.12) is that a large r reduces the absolute values of λ_1 and α is in an reduced magnitude. In addition,

the two values are related by the constant coefficient $I = 1 + b + \sigma = -(\lambda_1 + 2\alpha) < 0$. This makes the two in a comparable scale to reinforce the canceling effect that leads to the trivial oscillation magnitude. It is apparent that the characteristics of the eigenvalues offers a compelling argument for the homoclinic explosions at a large r.

5. Discussions and conclusions

Our bifurcation analysis and the computation results indicate that the thermally induced convection flow presents drastically different behaviors when the transient thermal field drives the flow. The transient form Lorenz model incorporates the influence of the conductive layer and the heat transfer boundary condition for the flow behavior of the entire 2D field. The transient thermal field function influences the steady-state and transient oscillations. We identified stationary steady-state attractors that exist subject to certain transient thermal field functions. The fluctuation of the thermal field modifies the attractors, bifurcation conditions for the initiation of the unstable flow. It also affects the bursts of the homoclinic bifurcation, though not the homoclinic orbit itself. The transient thermal field variation is likely to cause transitions among different bifurcation behaviors, which could generate turbulence or chaos due to instantaneous transitions of the attractors.

The bifurcation analysis from this study provides a quantified justification for the sequential bifurcations at different thermal and fluid parameters. This explains the successive bifurcations exhibited by the original Lorenz model as well as the current model at a different range of parameters. Further, we identified the mechanisms of the bursts of the homoclinic explosions at a large r. We attribute the explosions to the trivial effect of the oscillation amplitude determined by these eigenvalues at large r that is sensitive to numerical computation errors to alter the oscillation orbits.

This study revealed the typical behaviors of the thermally induced convection flow with a transient thermal source and predicted the system response in both qualitative and quantitative terms for the bifurcations of steady-state attractors. These bifurcation conditions shed light on the turbulence of the thermally induced convection flow.

Nomenclature

a: critical wave number
b: geometry factor
c: geometry factor
d: coefficient for the thermal boundary condition effect
d_N, d_D: coefficients d for the Newmann and Dirichlet condition, respectively
e_κ: coefficient for the thermal diffusivity between the fluid and the solid
$f^-_{\text{sup}}(r)$: necessary condition for the supercritical Hopf bifurcation with $\lambda_1 < 0$
$f^-_{\text{sub}}(r)$: necessary condition for the subcritical Hopf bifurcation with $\lambda_1 < 0$
$f^+_{\text{sub}}(r)$: necessary condition for the subcritical Hopf bifurcation with $\lambda_1 > 0$
$f^*_H(r)$: necessary and sufficient condition for the Hopf bifurcation with a specified eigenvalue $\lambda_1 > 0$ or $\lambda_1 < 0$

fsd: bifurcation curve for the Hopf bifurcation with the concurrent saddle node bifurcation

fpd: bifurcation curve for the Hopf bifurcation with the concurrent period doubling bifurcation

fHp: bifurcation curve for the subcritical Hopf bifurcation at $\lambda_1 = 15$

fHn: bifurcation curve for the Hopf bifurcation at $\lambda_1 = -15$

$fh > 0$: the contour projection of the function $f_{\text{sub}}^{-}(r) > 0$

$fnh > 0$: the contour projection of the function $f_{nh}(r) > 0$

$f \text{ sub } p > 0$: curve for the contour projection of the function $f_{\text{sub}}^{+}(r) > 0$

g: gravitational acceleartion

$g_T(t)$, $g_T(\tau)$: transient thermal field function

$g_{T,\tau}(\tau)$: time derivative of the transient thermal field function $g_T(\tau)$

H: height of the fluid cell

I, II, III: coefficients

J: Jocobi of the system

L: length of the fluid cell

r: ratio between R_a and R_c

r^*: threshold value of r for $r > 0$

R_a: Rayleigh number

R_c: critical Rayleigh number

$T(x,z,t)$: temperature of the flow field

T_0: magnitude of the temperature variation at the bottom layer

$T_1(x,z,t)$: linear temperature variation along z

$\Delta T(x,0,t)$: temperature difference between the two parallel plates

X: variable for the function $\theta_{11}(x,z,t)$

Y: variable for the function $\theta_{02}(x,z,t)$

Z: variable for the function $\psi(x,z,t)$

u, w flow in x and z, respectively

ε: the coefficient of volume expansion of the fluid

α: the real part of the eigenvalue

γ: the imaginary part of the eigenvalue

$\beta(\tau)$: ratio between $g_{T,\tau}(\tau)$ and $g_T(t)$

δ: intermediate variable

κ: thermal diffusivity of fluid

κ_L: thermal diffusivity of solid at the bottom plate

σ: Prandtl number

η: intermediate variable

λ: eigenvalue

τ: normalized time

ω: frequency of the transient thermal field function

θ, θ_{11}, θ_{02}: temperature variation of the flow field

ν: kinematic thermal viscosity

$\psi(x,z,t)$: flow field stream function

Δ_{nh}: operator for the attractors when the eigenvalues are real or complex

Δ_H^-: operator for the attractor at the Hopf bifurcation with $\lambda_1 < 0$

Δ_{sub}^+: operator for the attractor at the Hopf bifurcation with $\lambda_1 > 0$

Δ_H^*: operator for the attractor at the Hopf bifurcation with a specified λ_1

References

[1] E. N. Lorenz, "Deterministic nonperiodic flow," *Journal of the Atmospheric Sciences*, vol. 20, no. 2, pp. 130–141, 1963.

[2] B. Saltzman, "Finite amplitude free convection as an initial value problem—I," *Journal of the Atmospheric Sciences*, vol. 19, no. 4, pp. 329–341, 1962.

[3] L. Rayleigh, "On convection currents in a horizontal layer of fluid, when the higher temperature is on the other side," *Philosophical Magazine and Journal of Science*, vol. 32, pp. 529–546, 1916.

[4] J. A. Yorke, E. D. Yorke, and J. Mallet-Paret, "Lorenz-like chaos in a partial differential equation for a heated fluid loop," *Physica D*, vol. 24, no. 1–3, pp. 279–291, 1987.

[5] A. C. Fowler and M. J. McGuinness, "A description of the Lorenz attractor at high prandtl number," *Physica D*, vol. 5, no. 2-3, pp. 149–182, 1982.

[6] E. J. Kostelich and J. A. Yorke, "Lorenz cross sections of the chaotic attractor of the double rotor," *Physica D*, vol. 24, no. 1–3, pp. 263–278, 1987.

[7] E. N. Lorenz, "The local structure of a chaotic attractor in four dimensions," *Physica D*, vol. 13, no. 1-2, pp. 90–104, 1984.

[8] D. D. Joseph, "On the stability of the Boussinesq equations," *Archive for Rational Mechanics and Analysis*, vol. 20, no. 1, pp. 59–71, 1965.

[9] J. Guckenheimer, "Sensitive dependence to initial conditions for one dimensional maps," *Communications in Mathematical Physics*, vol. 70, no. 2, pp. 133–160, 1979.

[10] J. Guckenheimer, "A strange, strange attractor," in *The Hopf Bifurcation and Its Applications*, J. E. Marsden and M. McCracke, Eds., vol. 19 of *Applied Mathematical Science*, pp. 368–381, Springer, New York, NY, USA, 1976.

[11] C. Sparrow, *The Lorenz Equations: Bifurcations, Chaos, and Strange Attractors*, vol. 41 of *Applied Mathematical Sciences*, Springer, New York, NY, USA, 1982.

[12] J. B. McLaughlin and P. C. Martin, "Transitions to turbulence in a statistically stressed fluid system," *Physical Review A*, vol. 12, no. 1, pp. 186–203, 1975.

[13] J. B. McLaughlin, "Successive bifurcations leading to stochastic behavior," *Journal of Statistical Physics*, vol. 15, no. 4, pp. 307–326, 1976.

[14] J. H. Curry, "Chaotic response to periodic modulation of model of a convecting fluid," *Physical Review Letter*, vol. 43, no. 14, pp. 1013–1016, 1979.

[15] J. H. Curry, "A generalized Lorenz system," *Communications in Mathematical Physics*, vol. 60, no. 3, pp. 193–204, 1978.

[16] C. Boldrighini and V. Franceschini, "A five-dimensional truncation of the plane incompressible Navier-Stokes equations," *Communications in Mathematical Physics*, vol. 64, no. 2, pp. 159–170, 1979.

[17] V. Franceschini and C. Tebaldi, "Sequences of infinite bifurcations and turbulence in a five-mode truncation of the Navier-Stokes equations," *Journal of Statistical Physics*, vol. 21, no. 6, pp. 707–726, 1979.

[18] J. D. Gibbon and M. J. McGuinness, "The real and complex Lorenz equations in rotating fluids and lasers," *Physica D*, vol. 5, no. 1, pp. 108–122, 1982.

Xiaoling He: Department of Materials Engineering, College of Engineering and Applied Science, University of Wisconsin-Milwaukee, 3200 North Cramer Street, P.O. Box 784, Milwaukee, WI 53201-784, USA
Email address: xiaoling@uwm.edu

Advances in Difference Equations

Special Issue on Boundary Value Problems on Time Scales

Call for Papers

The study of dynamic equations on a time scale goes back to its founder Stefan Hilger (1988), and is a new area of still fairly theoretical exploration in mathematics. Motivating the subject is the notion that dynamic equations on time scales can build bridges between continuous and discrete mathematics; moreover, it often revels the reasons for the discrepancies between two theories.

In recent years, the study of dynamic equations has led to several important applications, for example, in the study of insect population models, neural network, heat transfer, and epidemic models. This special issue will contain new researches and survey articles on Boundary Value Problems on Time Scales. In particular, it will focus on the following topics:

- Existence, uniqueness, and multiplicity of solutions
- Comparison principles
- Variational methods
- Mathematical models
- Biological and medical applications
- Numerical and simulation applications

Before submission authors should carefully read over the journal's Author Guidelines, which are located at http://www.hindawi.com/journals/ade/guidelines.html. Authors should follow the Advances in Difference Equations manuscript format described at the journal site http://www.hindawi.com/journals/ade/. Articles published in this Special Issue shall be subject to a reduced Article Processing Charge of €200 per article. Prospective authors should submit an electronic copy of their complete manuscript through the journal Manuscript Tracking System at http://mts.hindawi.com/ according to the following timetable:

Manuscript Due	April 1, 2009
First Round of Reviews	July 1, 2009
Publication Date	October 1, 2009

Lead Guest Editor

Alberto Cabada, Departamento de Análise Matemática, Universidade de Santiago de Compostela, 15782 Santiago de Compostela, Spain; alberto.cabada@usc.es

Guest Editor

Victoria Otero-Espinar, Departamento de Análise Matemática, Universidade de Santiago de Compostela, 15782 Santiago de Compostela, Spain; mvictoria.otero@usc.es